

Simulation of Evacuated Tube Collector and Storage of Hybrid Air-conditioning System

Mustafa Ahmed Abdulhussain

Mechanical Engineering Department ,University of Technology

mustafa.ahmed1971@gmail.com

Abstract

The CFD transient simulation of superheating the refrigerant R410 through the heat exchange with the evacuated tube water heating system of the hybrid split air conditioner that is subjected to solar radiation of constant intensity with the contribution of fan accelerated air is performed by the ANSYS-CFX code. The comparison with experimental work showed a minimum percentage error 8% of the predicted refrigerant evaporative heat transfer with storage tank horizontal tubing. In addition, the results denoted high absorption rate for the evacuated tubes, reducing highly reversed heat transmission for the circulated water.

Keywords: Hybrid, Solar assisted, Evacuated tubes, Air conditioner.

الخلاصة

تم اجراء محاكاة عددية لنمذجة التسخين الاضافي الانتقالي لمائع التبريد R410 من خلال التبادل الحراري مع الماء المسخن في الانابيب الزجاجية المفرغة في الوحدة الخارجية لمكيف هواء هجين معرض لاشعاع شمسي ثابت الشدة مع مساهمة حركة الهواء المتسارع عبر مروحة المكثف باستخدام برنامج ANSYS-CFX. اظهرت المقارنة مع النتائج العملية نسبة خطأ 8% لمعامل انتقال الحرارة التبخيري لمائع التبريد مع جدران انبوب خزان الماء. اضافة الى ذلك اظهرت النتائج نسبة امتصاص عالية للانابيب الزجاجية مما يقلل الانتقال العكسي للحرارة من الماء المسخن الى الخارج بوجود هواء متسارع

الكلمات المفتاحية: مكيف هواء هجين، شمسي مساعد، انابيب مفرغة.

Nomenclature			Greek symbols		
Symbol	Definition	Unit	Symbol	Definition	Unit
u, v, w	Polar velocity component	m/sec	μ	Dynamic viscosity	kg/m.sec
C_p	specific heat	KJ/kg. °C	ρ	Density	kg/m ³
h	Enthalpy	KJ/Kg	$\sigma_k, \sigma_\epsilon, c_1, c_2$	Turbulent model empirical constants	-
H	Convection heat transfer	W/m ² K	ϵ	Rate of dissipation of kinetic energy	J/kg.sec
P	Pressure	Pa	Subscript	Definition	
T	Temperature	°C	x, y, z	Cartesian velocity sub-component	
t	Time	minute			

1. Introduction

The efficient utilization of evacuated tubes for solar heating due to their low heat loss coefficient and high absorption rate has led to their adoption as a second stage of refrigerant compression in the split-type air conditioning systems especially for solar radiation regions. The main benefit of this technology is to reduce energy consumption via condenser heat sink temperature increasing resulting in compressor load reduction. Figure (1) shows a schematic diagram of the hybrid solar-assisted air conditioning cycle in which the refrigerant after the compression is heat exchanged with the evacuated tubes collector fluid (water liquid) resulting in an additional superheating degree, then it continues to its ordinary cycle stages, condensing, thermal expansion, and evaporating. (Kumar *et.al.*, 2016) analyzed the performance characteristics of the hybrid system working with R-410a under different operating conditions experimentally. The analysis comprises the COP, evaporator cooling capacity, and compressor plus condenser inlet and outlet refrigerant temperature as well as the water temperature difference. Evaporator supplied air conditions such as relative humidity and dew point temperature have been analyzed. The main results showed that this system has an improved efficiency with higher COP when the evacuated tubes were exposed directly to sunlight (Bouraba *et.al.*, 2017) performed a theoretical study of the solar-assisted air conditioning performance comparison with three refrigerants R134a, R410a and R1234 ze (E) based on their Pressure-Enthalpy charts, they investigated the effect of Refrigerant outlet temperature leaving the solar collector storage tank on the system COP, the energy conservation gain on compressor load and the condensation required heat exchanged surface areas assuming equal cycle sub cooling and superheating degrees. They concluded that COP is the highest for R1234 ze (E) rather than R134a and R410a respectively as well as the gain in compressor load. R1234 ze (E) requires a larger condensing surface area due to its highly heat absorption from storage tank which increases with its increased temperature. An experimental data acquisition sensing analysis has been implemented on the same system by (Vakiloroaya *et.al.*, 2013) at steady state condition, the effect of water temperature, storage tank size and air-conditioned room desired temperature on the system energy consumption have been studied. The compressor increased off-duty time leads to monthly saving of 25-42% were the major important result.

(Hussain *et.al.*, 2017) investigated experimentally and analytically the performance operation of the hybrid system in Iraq hot weather conditions, they compared the results with the conventional type air conditioner, the most remarkable results showed that the hybrid system have the same performance and the of power saving rate with the conventional type, the solar assisted system had a decreased condenser capacity and COP with respect to the conventional type air conditioner. (Laknizi *et.al.*, 2016) evaluated experimentally the evacuated tube hybrid A/C energy consumption under various weather condition in Morocco. Two cases were considered, the first with empty storage tank fluid and the second with a filled tank of water, liquid at (70°C), the system delivered cooled room enclosure of about (20-22°C) and relative humidity (40-65%). The maximum energy saving can reach 88 KWA/year for a 6-month running continuously at a maximum ambient temperature of (38°C). In order to increase the refrigerant sub cooling degree in the hybrid system, an enhanced control system developed by (Vakiloroaya *et.al.*, 2013) installed after the compression stage consists of a by-pass line with solenoid valve controlled by a linear quadratic regulator that controls the refrigerant flow rate by sensing Freon entering temperature to the condenser in transient condition. The system gives very high efficiency contributes to better refrigeration effect. An additional factor has been integrated in the above-mentioned research is the condenser fan speed done by (Ha and Vakiloroaya, 2014). A

better energy saving rate for the control system with a maximum of (7%) have been achieved. Several researchers have made a CFD simulation of evacuated tube solar collector. (Ayala *et.al.*, 2015) predicted the temperature contours in the collector exit manifold at steady state conditions using the Boussinesq and the variable temperature water properties approaches. They concluded that the Boussinesq method is better in accuracy with experimental data. (Paradis *et.al.*, 2015) simulated the transient variation in the water mass flow rate, the ambient temperature, solar radiation and wind speed on the evacuated tube one-dimensional model solving using the Range-Kutta algorithm. The importance of higher incident radiation positive effect on water temperature and the adverse wind speed effect was the most concluded results. (Essa and Mostafa, 2017) simulated the three-dimensional model collector, the temperature variation and flow circulation in the evacuated tubes and storage tank were computed at the variable solar radiation intensity and incident angle using the discrete ordinates solar radiation model. They reached an average error with experiments of about (4-8%). In addition, they observed the flow, streamline shape forming two structures, one with a linear profile near the tube top surface and the other is helical inside the tube. A solar assisted heat pump system using the refrigerants R134 and R774 (carbon dioxide) have been analyzed experimentally by (Baradey *et.al.*, 2016) for different applications such as enclosure cooling and water heating, the carbon dioxide refrigerant R774 had achieved a greater improvement in system performance and energy consumption. (Jin *et.al.*, 2017) designed a novel storage multi tank system for the solar air conditioning units with highly cooling demands considering constant solar radiation load. They concluded that the system response with respect of number of tanks utilized could be improved (decreased) by about 7 hours when using four tank for filling and evacuation. Meanwhile, the number of tanks used have a minor effect on ideal water heating rate.

The aim of this research is to simulate numerically the incident radiation transient absorption rate by the evacuated tubes resulting in heating the water firstly, and secondly simulate the heat exchanged between the thermal insulated tank water and the refrigerant R410a piping flow. The simulation is performed on (12,000 BTU) split outdoor unit using the ANSYS-CFX code considering a constant subjected radiation intensity of 750 W/m^2 , the fan air flow leaving the condenser at climate conditions of (45°C). The outdoor unit body temperature set equal to the surrounding atmospheric enclosure. With transient periods of 1, 3, and 6 minutes, the solar collector plus the refrigerant thermal properties change will be observed.

2. CFD modelling

The above-described case simulation involves two different flow patterns, first the water circulation in the evacuated solar collector (tubes + tank) is considered laminar flow as the major factors of circulation is the buoyancy effect in addition to the fluid internal energy change (thermo-syphon phenomena) due to solar heating effect. Second, the turbulent flow pattern for the fan-accelerated airflow and the refrigerant flow turning through the storage tank.

The simulation modelling is performed by solving the continuity, momentum (Navier-Stokes) equations in X, Y, Z directions and the energy equations for the laminar and turbulent domains considering variable flow properties as follows:

The continuity equation

$$\frac{\partial(\rho u_x)}{\partial x} + \frac{\partial(\rho u_y)}{\partial y} + \frac{\partial(\rho u_z)}{\partial z} = 0 \quad (1)$$

The X-momentum equation

$$u_x \frac{\partial(\rho u_x)}{\partial x} + u_y \frac{\partial(\rho u_y)}{\partial y} + u_z \frac{\partial(\rho u_z)}{\partial z} = -\frac{\partial P}{\partial x} + \frac{\partial}{\partial x} \left\{ \mu \left[2 \frac{\partial u_x}{\partial x} - \frac{2}{3} \left(\frac{\partial u_x}{\partial x} + \frac{\partial u_y}{\partial y} \right) \right] \right\} + \frac{\partial}{\partial y} \left[\mu \left(\frac{\partial u_x}{\partial y} + \frac{\partial u_y}{\partial x} \right) \right] + \frac{\partial}{\partial z} \left[\mu \left(\frac{\partial u_x}{\partial z} + \frac{\partial u_z}{\partial x} \right) \right] \quad (2)$$

The Y-momentum eq.

$$u_x \frac{\partial(\rho u_y)}{\partial x} + u_y \frac{\partial(\rho u_y)}{\partial y} + u_z \frac{\partial(\rho u_y)}{\partial z} = -\frac{\partial P}{\partial y} + \rho g_y + \frac{\partial}{\partial y} \left\{ \mu \left[2 \frac{\partial u_y}{\partial y} - \frac{2}{3} \left(\frac{\partial u_x}{\partial x} + \frac{\partial u_y}{\partial y} \right) \right] \right\} + \frac{\partial}{\partial x} \left[\mu \left(\frac{\partial u_y}{\partial x} + \frac{\partial u_x}{\partial y} \right) \right] + \frac{\partial}{\partial z} \left[\mu \left(\frac{\partial u_y}{\partial z} + \frac{\partial u_z}{\partial y} \right) \right] \quad (3)$$

The Z-momentum eq.

$$u_x \frac{\partial(\rho u_z)}{\partial x} + u_y \frac{\partial(\rho u_z)}{\partial y} + u_z \frac{\partial(\rho u_z)}{\partial z} = -\frac{\partial P}{\partial z} + \frac{\partial}{\partial z} \left\{ \mu \left[2 \frac{\partial u_z}{\partial z} - \frac{2}{3} \left(\frac{\partial u_x}{\partial x} + \frac{\partial u_y}{\partial y} \right) \right] \right\} + \frac{\partial}{\partial x} \left[\mu \left(\frac{\partial u_z}{\partial x} + \frac{\partial u_x}{\partial z} \right) \right] + \frac{\partial}{\partial y} \left[\mu \left(\frac{\partial u_z}{\partial y} + \frac{\partial u_y}{\partial z} \right) \right] \quad (4)$$

The Energy equation

$$u_x \frac{\partial(\rho c_p T)}{\partial x} + u_y \frac{\partial(\rho c_p T)}{\partial y} + u_z \frac{\partial(\rho c_p T)}{\partial z} = \frac{\partial}{\partial x} \left(k \frac{\partial T}{\partial x} \right) + \frac{\partial}{\partial y} \left(k \frac{\partial T}{\partial y} \right) + \frac{\partial}{\partial z} \left(k \frac{\partial T}{\partial z} \right) \quad (5)$$

The scalable K-ε turbulence model for the turbulent flow of air and Refrigerant are as follows

$$\begin{aligned} \frac{\partial(\rho k)}{\partial t} + \nabla \cdot (\rho U K) &= \nabla \cdot \left[\left(\mu + \frac{\mu}{\sigma_k} \right) \nabla K \right] + P - \rho \epsilon \\ \frac{\partial(\rho \epsilon)}{\partial t} + \nabla \cdot (\rho U \epsilon) &= \nabla \cdot \left[\left(\mu + \frac{\mu}{\sigma_\epsilon} \right) \nabla \epsilon \right] + \frac{\epsilon}{k} (c_1 P - c_2 \rho \epsilon) \end{aligned} \quad (6)$$

2.1 Geometry meshing

The hybrid-solar assisted A/C outdoor unit shown in figure (2) was sketched using the SOLIDWORKS 2016 software. It consists of 10 evacuated tubes with a storage tank mounted on the condensing unit; the cooling air from the back face is accelerated through the axial fan then passes towards the evacuated tubes, which are full of circulating hot water. The geometry is transferred to the ANSYS-CFX package for simulation.

The simulation modelling of the problem has two challenges that are the thermal interference of the incident solar radiation on the tubes with the relatively hot air passing through. In addition, the rate of water heating due to the prescribed subjected load resulting into R410 heat exchange with circulating flow.

The first step of solving is to mesh the geometry with the tetrahedrons non-uniform method with is shown in figure (3a) considering default mesh characteristics of curvature minimum angle (18°), the mesh faces and cells minimum and maximum sizes taken around (7e-4&7e-2) respectively. The mesh statistics exceeded 48000 nodes with 1750000 cells.

2.2 Applied boundary conditions

In order to perform the solution, the dented figures (3b&c) and table (1) shows the applied boundary conditions to the geometry considering transient case conditions:

- 1- The condensing unit outer surface of the A/C is assumed to have the environment temperature at beginning of operation, thus its convective heat transfer will be neglected.
- 2- Solar radiation of fixed intensity (750 W/m^2) treated as a heat flux is applied to the evacuated tubes outer surface, which will be absorbed through the inner thickness and the vacuum layer and the thermal coating reaching the water domain with applying the atmospheric open boundary condition for the tank.
- 3- The air passing the condensing unit is considered as a heated domain that is heat exchanged with condensed Refrigerant enters the moving fan boundary with (45°C) and accelerated with (500-RPM) angular velocity passing around the solar collector with atmospheric pressure condition.
- 4- Accelerated airflow forced convection heat transfer coefficient with evacuated tubes was taken according to (Paradis *et.al.*, 2015) at an average of ($50 \text{ W/m}^2\text{K}$).
- 5- The refrigerant R410 velocity magnitude should not less than (5m/Sec) in vertical tubes after compressor discharge with operating pressure (16 bar) according to (Laknizi *et.al.*, 2016) to ensure oil circulation where it flows through vertical piping from the compressor to the water tank. Taking into consideration copper piping of Freon with (2mm) thickness subjected to convection heat transfer inside the storage tank. Since the refrigerant have considered a superheated vapor from compressor output. (Greco and Vanoli, 2005) predicted the evaporation heat transfer coefficient range in the horizontal tube for R410 between ($4000\text{-}8000 \text{ W/m}^2\text{K}$), to achieve minimum percentage error with experiments. Several runs have been executed within the limit values described to obtain the desired result.
- 6- The Freon entering initial temperature was taken equal to the measured value taken by (Laknizi *et.al.*, 2016), also Water circulation inside solar collector is considered laminar, a mean value of ($600 \text{ W/m}^2\text{K}$) convectional heat transfer calculated numerically by (Liang *et.al.*, 2011) have been adjusted for the solution.

2.3 Imitation procedure

The transient behavior of the case has been simulated for three-time periods: 1, 3 and 6 minutes in consideration of computer hardware limitations the time step for each iteration taken as (0.5 Sec). The objective of the modelling is to show the heat transmission across the circulated water due to solar load and its influence on the Freon additional heating, also, the heat gain enclosure of fan-accelerated airflow due to the applied solar radiation is imitated.

3. Results and conclusions

3.1 Solar collector:

the transient results shown in figures (4, 5 and 6) a gradual rise in circulating water temperature along the evacuated tubes and in the storage tank remarking the partial sub-cooling effect of fan accelerated air, especially for the (1) minute time period. At the time undergoes further, the solar radiation becomes more effective and the water heat gain becomes the major resultant noticing gradual rise in water minimum temperature as the time of imitation increases. The air velocity vector change due to the fan rotation is observable in figure (7)

The cross-sectional view of the flow domain in the collector clarified in figures (8, 9 and 10) demonstrates the local gradual water thermal state change remarking the maximum temperature contour is the closest to the evacuated tube inner surface at the (1) minute case where the higher water temperature contour exists at the upper storage tank region noticing that the circulating water flow gradual stepped change from the outer tubes surface to the inner core

area as viewed in figure (8). As a conclusion the effect the crossed air flow partial subcooling effect is significant at this time period.

Figures (9&10) indicates the stepped local heating contours perception remarking the accumulation solar radiation effect on water temperature rising especially at the middle and bottom tubes sections. In addition, the filled tank water tends towards the uniformity and the stability condition as the simulation time undergoes further. In figures (9&10), the gravity effect on the heat-accumulated flow is perspicuous, the resulting contour signifies the gradual thermal integration between water circulation streamlines.

The water velocity variation along the time of imitation is presented in figures (11, 12 and 13) where a moderate rise in laminar flow maximum and minimum velocity contours occurs. In figure (11) when the time elapsed (1) minute, the flow is accelerated slightly due to the rise in its kinetic energy as it flows down in the tube, then a mixing zone is generated near the neck of the tube and in the storage tank. When the time is passing, the momentum exchange will arise resulting in more flow circulating acceleration and larger flow disturbances in the storage tank as illustrated in figures(12&13)

3.2 Refrigerant flow

In order to evaluate the R410 superheating degree, it is necessary to predict the convection heat transfer coefficient value considering superheated vapor as the inlet condition. As described in the application of boundary conditions, a comparison with achieving experimental results done by (Kumar *et.al.*, 2016) through an evaluation of fluid enthalpy change across the horizontal tube to predict the optimum heat transfer value within the estimated range evaluated by (Greco and Vanoli. 2005).

Many solution iterations have been performed at different heat transfer values (4000-8000 W/m²K), the change in the maximum enthalpy difference between inlet and exit flow error rate with experiments is configured in figure (14) which clearly indicates a minimum error of about (8%) is present when $H=4600$ W/m²K.

This result has been approved in the evaluation of refrigerant temperature transient rise at the specified time intervals as observed in figures (15, 16 and 17) which indicates the gradual stepped up R410a vapor superheating reaching 7°C at 6 minutes time interval.

3.3 Conclusions:

The most important derivation is that the evacuated tubes have a high absorptivity rate due to the twin layered glass with an enclosed in-between cavity that prohibits the back-heat flow outwards the heated circulated water domain. The anticipation of R410 evaporative heat transfer coefficient across the storage tank copper tube fulfilled a stable Refrigerant transient superheating that reaches maximum of 7°C for a transient time 6 minutes.

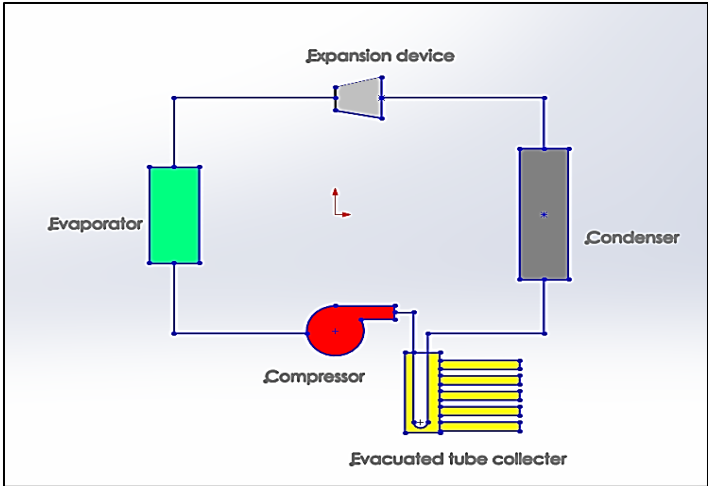


Figure (1) hybrid Refrigeration cycle

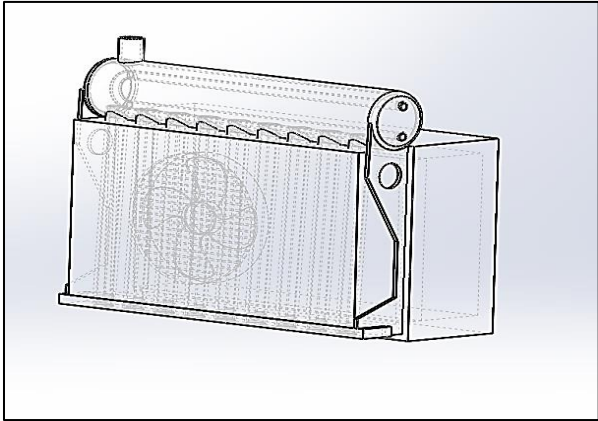


Figure (2) the hybrid solar-assisted outdoor unit

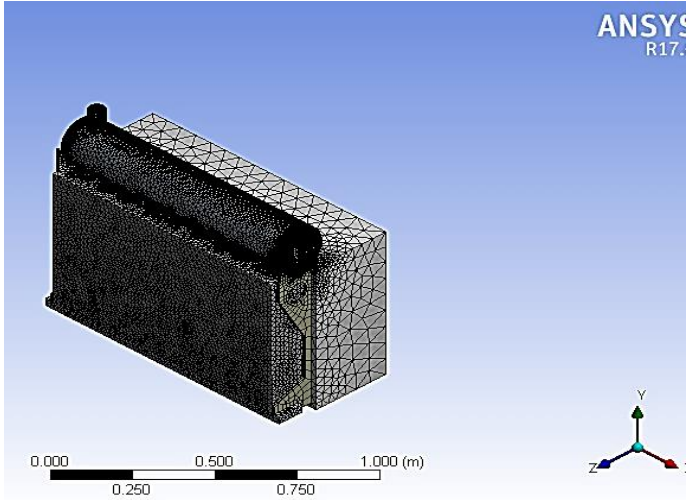
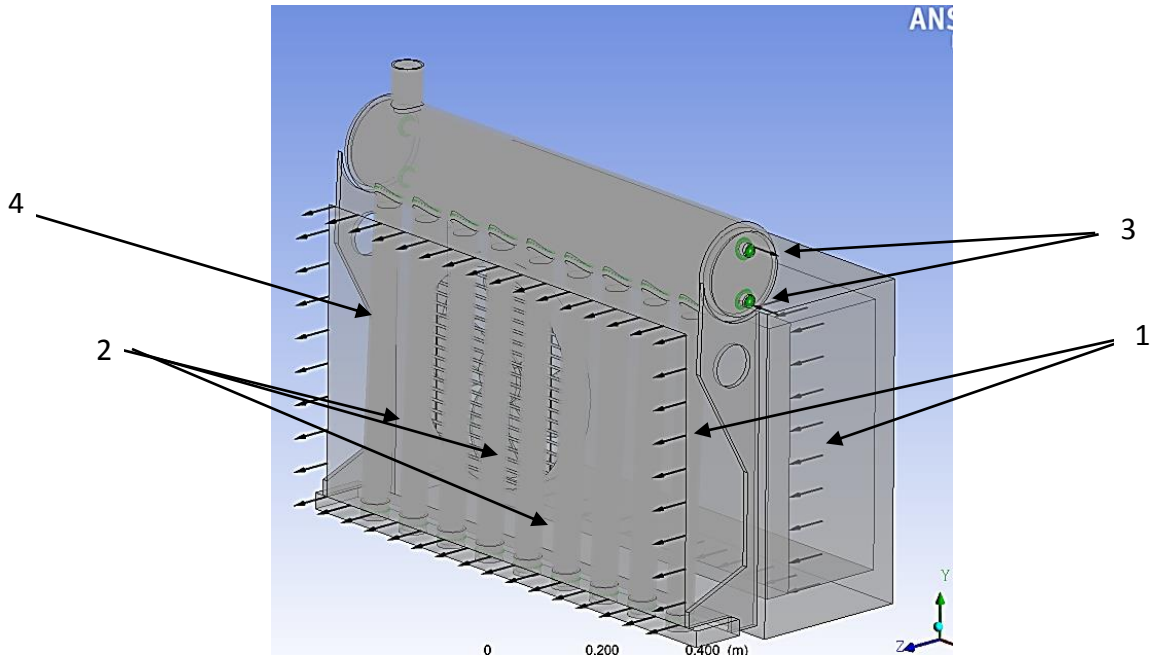
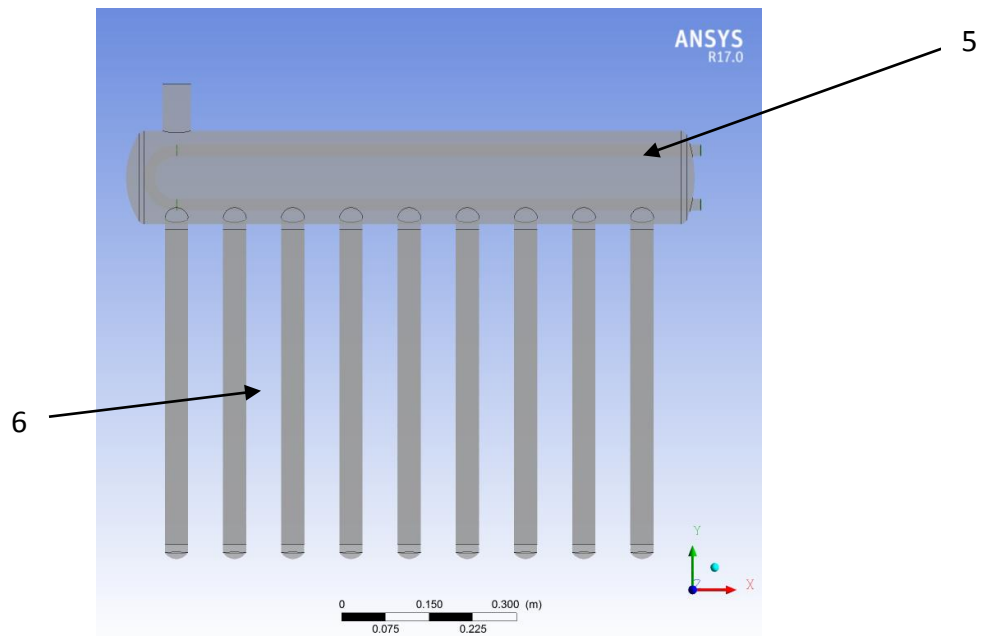


Figure (3a) the geometry meshing



Figures (3b) applied boundary conditions



Figures (3c) applied boundary conditions

Encoding	Clarification	Value
1	Air flow inlet and exit conditions	$V_{in}=2$ m/sec, $T_{in}=45^{\circ}\text{C}$, $P_{out}=1$ atm
2	subjected solar heat flux on outer tubes surfaces	$I=750$ W/m^2
3	Refrigerant inlet and exit conditions	$V_{in}=5$ m/sec, $T_{in}=40^{\circ}\text{C}$, $P_{out}=16$ bar
4	Accelerated flow with evacuated tubes convection heat transfer coefficient	$h=50$ $\text{W/m}^2\text{K}$
5	Refrigerant to copper tube forced convection heat transfer coefficient	Specified range as illustrated in figure (14)
6	Circulated water with evacuated tubes convection heat transfer coefficient	$h=600$ $\text{W/m}^2\text{K}$

Table (1) boundary conditions briefing

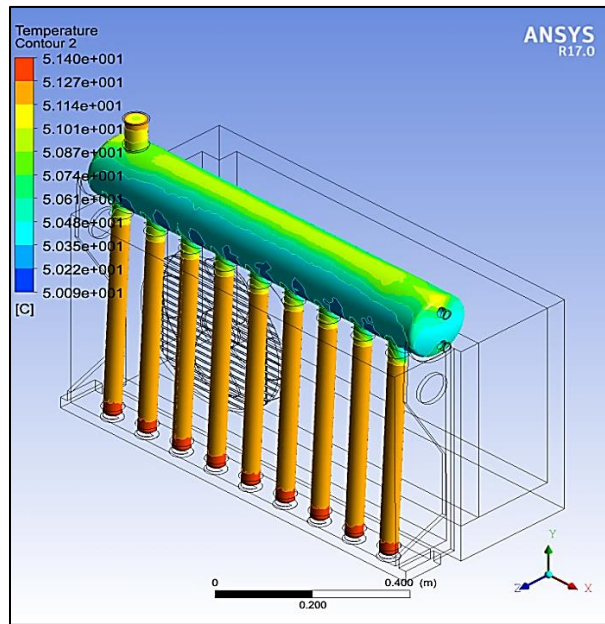


Figure (4) water solar heating effect at 1-minute period

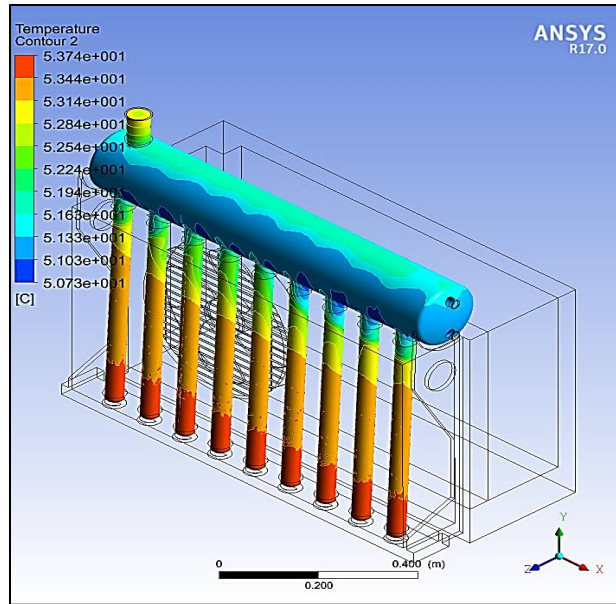


Figure (5) water solar heating effect at 3-minute period

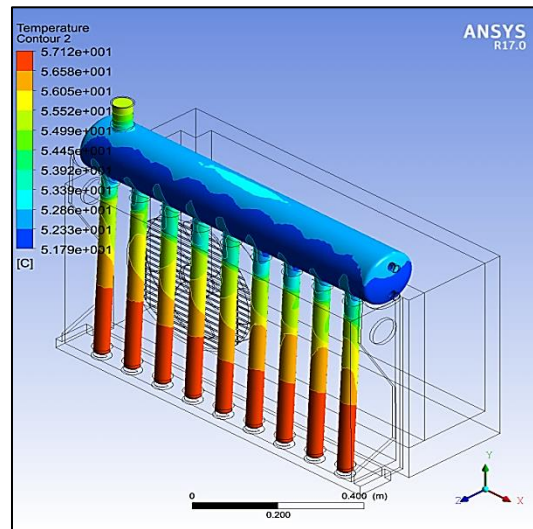


Figure (6) water solar heating effect at 6-minute period

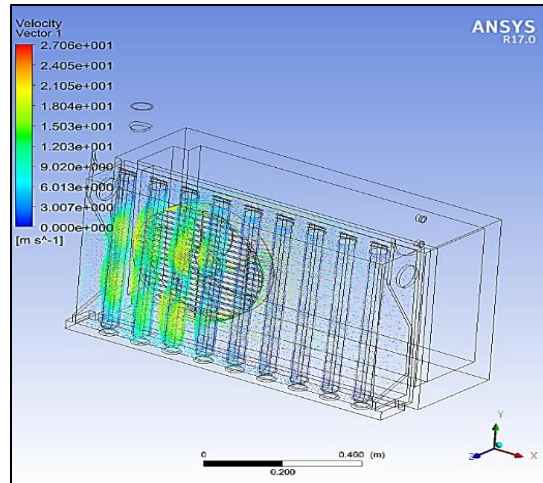


Figure (7) fan air streamline acceleration

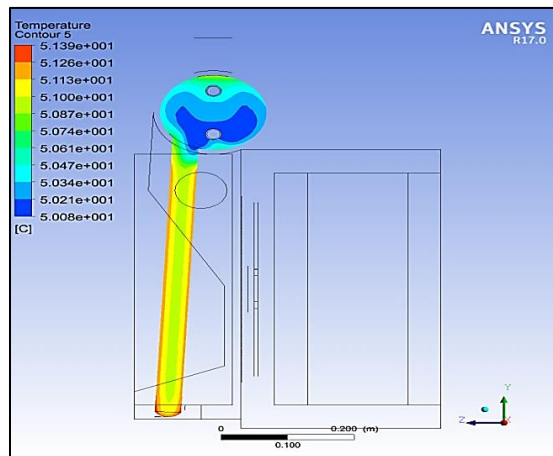


Figure (8) water cross sectional temperature contour at 1-minute period

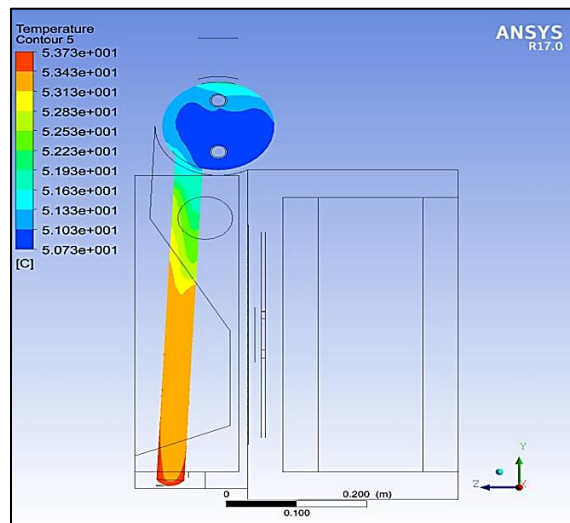


Figure (9) water cross sectional temperature contour at 3-minute period

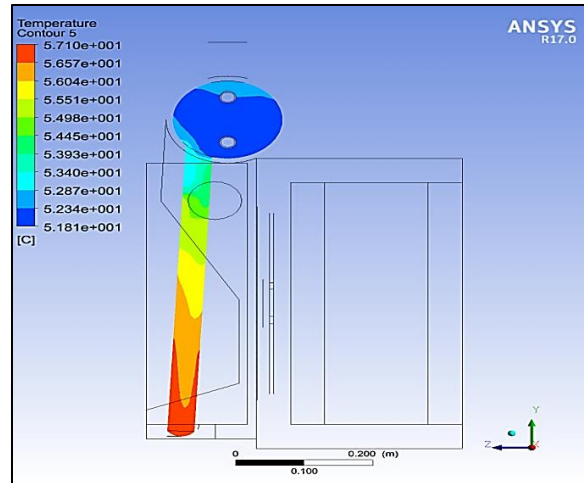


Figure (10) water cross sectional temperature contour at 6-minute period

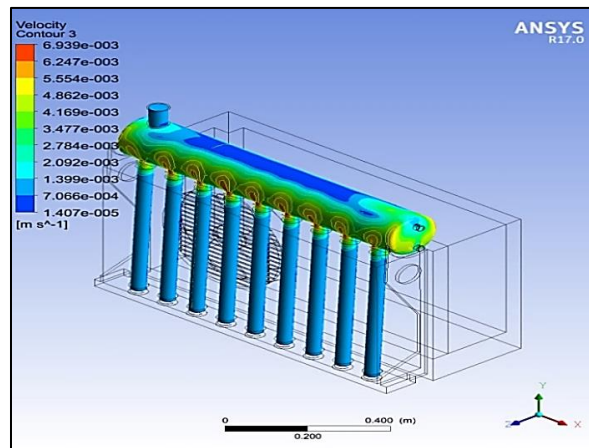


Figure (11) water velocity distribution at 1-minute period

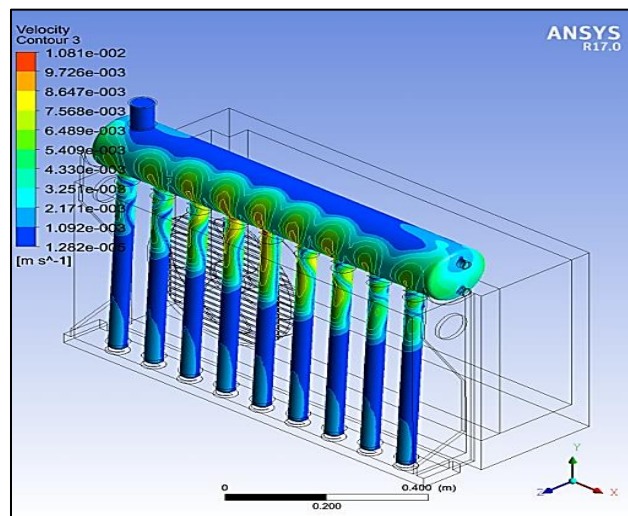


Figure (12) water velocity distribution at 3-minute period

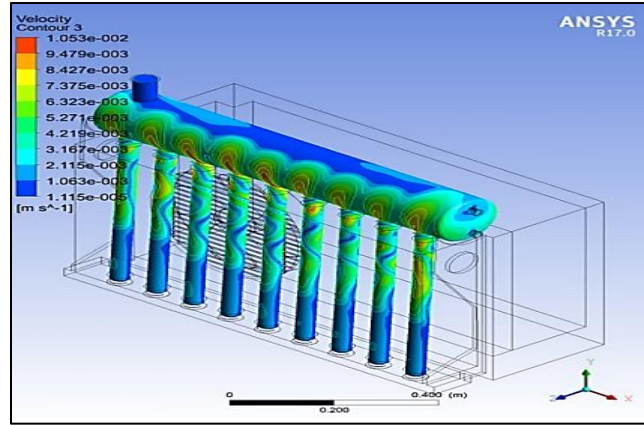


Figure (13) water velocity distribution at 6-minute period

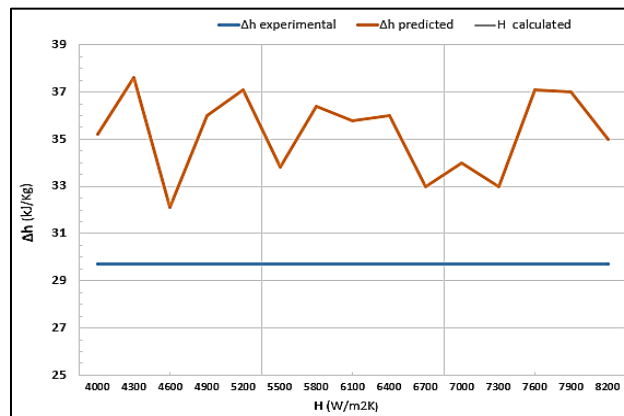


Figure (14) executional result for R410 enthalpy change with assigned convection heat transfer coefficient as compared with (Kumar *et.al.*,2016)

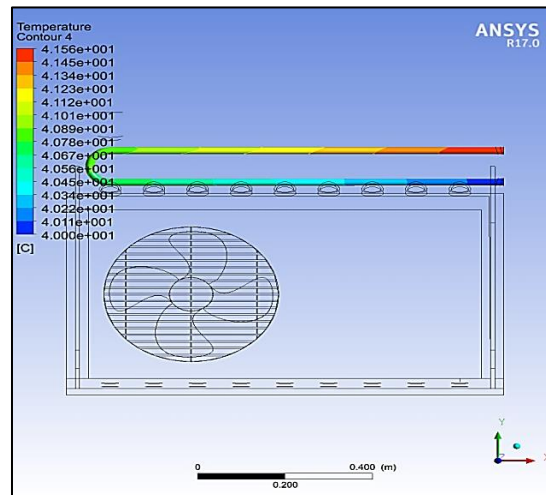


Figure (15) R410 temperature contour inside the water tank at 1 minute

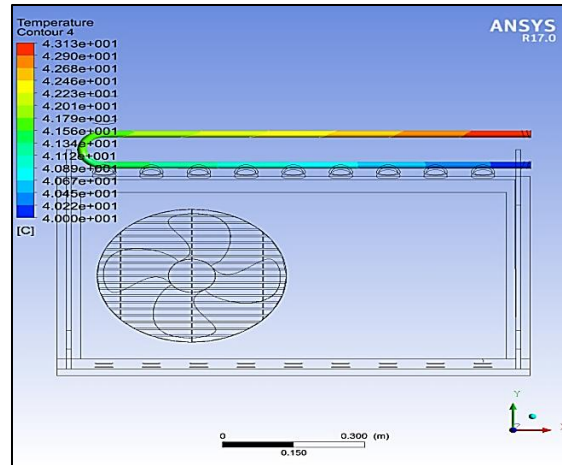


Figure (16) R410 temperature contour inside the water tank after 3 minutes

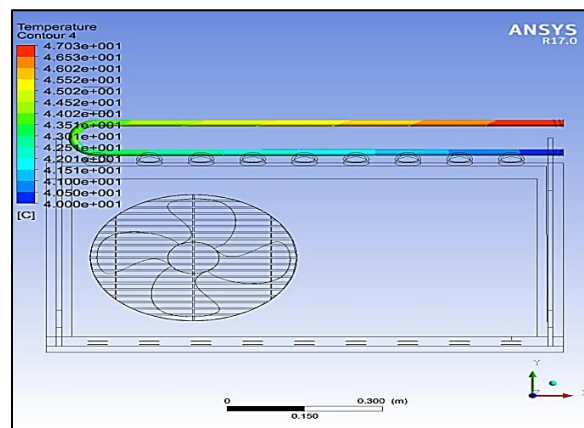


Figure (17) R410 temperature contour inside the water tank after 6 minutes

References:

- Ayala J. A. A.-, Rodríguez G. M.-, Núñez M P.-, Ramírez A. R. U. -and Muñoz A. G. -, 2015, "Numerical study of a low temperature water-in-glass evacuated tube solar collector", Energy Conversion and Management Journal, Vol.94, pp:472-481.
- Baradey Y., Hawlader , Ismail A.F. and Hrairi M.,2016 ,” Comparative Study of R134a and R744 Driven Solar Assisted Heat Pump Systems for Different Applications”, International Conference on Mechanical, Automotive and Aerospace Engineering.
- Bouraba A., Saighi M., Saidani-Scott H. and Hamidat A.,2017,” Cooling mechanism of a solar assisted air conditioner, an investigation based on pressure-enthalpy chart” International Journal of Refrigeration, Vol.80, pp: 274-291.
- Essa M. A. and Mostafa N. H., 2017,” Theoretical and experimental study for temperature distribution and flow profile in all water evacuated tube solar collector considering solar radiation boundary condition”, Solar Energy J., Vol. 142, pp: 267-277.
- Greco A. and Vanoli G, P.,2005, “Flow-boiling of R22, R134a, R507, R404A and R410A inside a smooth horizontal tube” International Journal of Refrigeration, Vol.28, pp:872-880.
- Ha Q. P., and Vakiloroyaya V., 2015,” Modeling and optimal control of an energy-efficient hybrid solar air conditioning system”, Automation in Construction J., Vol.49B, pp: 262-270.

- Hussain H. M., Habeeb L. J. and Abbas O. J.,2017," Investigation on Solar Hybrid Cooling system with High Latent Cooling Load", Advances in Environmental Biology J.,vol.11, Iss.4, pp.24-36.
- Jin S., Chen L. and Bu G.,2017," Experimental Investigation of a Novel Multi-Tank Thermal Energy Storage System for Solar-powered Air Conditioning", Applied Thermal Engineering, vol. 123, pp.953-962.
- Kumar S., Buddhi D., and Singh H. K., 2016," Performance Analysis of Solar Hybrid Air-Conditioning System with Different Operating Conditions", Imperial Journal of Interdisciplinary Research (IJIR), Vol.2, Iss.10, pp: 1951-1956.
- Laknizi A., Bouya M. and Ben Abdellah A., 2016," Evaluation of a domestic hybrid solar air conditioner system under various climate conditions", 2016 International Renewable and Sustainable Energy Conference (IRSEC).
- Liang R., Ma L., Zhang J., and Zhao D., 2011," Theoretical and experimental investigation of the filled-type evacuated tube solar collector with U tube", Solar Energy J., Vol. 85, pp: 1735-1744.
- Paradis P. L., Rouse D. R., Halle S., Lamarche L., and Quesada G., 2015," Thermal modeling of evacuated tube solar air collectors", Solar Energy J., Vol. 115, pp: 708-721.
- Vakiloroayaa V., Ha Q.P. and Skibniewski M., 2013," Modeling and experimental validation of a solar-assisted direct expansion air conditioning system", Energy and Buildings J., Vol. 66, pp: 524-536.